ELSEVIER

International Journal of Mass Spectrometry 207 (2001) 111–122

International Journal of Mass Spectrometry

Effectiveness of atomic and polyatomic primary ions for organic secondary ion mass spectrometry

Chris W. Diehnelt, Michael J. Van Stipdonk, Emile A. Schweikert*,[1]

Center for Chemical Characterization and Analysis, Department of Chemistry, Texas A&M University, College Station, TX, 77843-3144, USA

Received 1 September 2000; accepted 24 October 2000

Abstract

With the increased application of polyatomic primary ions for organic secondary ion mass spectrometry, a method to compare the performance of the various available projectiles is needed. In this work, primary ion performance was evaluated based on analyte-specific secondary ion yield, the amount of fragmentation, and the amount of metastable decay induced by each primary ion. These measurements were used to construct a projectile efficiency number for each primary ion applied to a specific analyte. An organic acid, phospholipids, and alkyl sulfates, prepared as multilayer and monolayer surfaces were analyzed with various atomic and polyatomic primary ions. It was found that polyatomic primary ions are best suited for multilayer organic samples whereas atomic primary ions are most effective for monolayer organic samples. Results are compared to other studies that measure the ion formation efficiency of various primary ions. (Int J Mass Spectrom 207 (2001) 111–122) © 2001 Elsevier Science B.V.

Keywords: Secondary ion mass spectrometry; Polyatomic primary ions; Desorption; Metastability

1. Introduction

Secondary ion mass spectrometry (SIMS) is utilized extensively in the analysis of surface organic and inorganic species [1]. Despite its success as a surface probe, the application of SIMS is often limited by the low secondary ion yields produced by atomic ion impacts. One approach to improve the secondary ion yield is to replace atomic primary ions with polyatomic primary ions [2–17]. For organic samples, large increases in the yield of molecular ions and sample specific ions are observed for samples bombarded with polyatomic ions. However, polyatomic primary ions have also been shown to increase prompt fragmentation [9] as well as the yield of nonspecific carbon clusters [18,19]. Additional work has shown that the disappearance cross section is higher, indicating a larger portion of the surface is disrupted by ion impact, when polyatomic primary ions are used [20–22]. Therefore, there is a tradeoff when using cluster projectiles; clusters produce high secondary ion yields but also induce more fragmentation, they disrupt a larger area of the surface, and they produce an increase in the amount of sample nonspecific peaks. In the context of chemical characterization, the issue is not simply to produce the maximum secondary ion

* Corresponding author. E-mail: schweikert@mail.chem.tamu.edu

[1] Present address: Department of Chemistry, Wichita State University, Wichita, Kansas 67260-0051, USA.

PII S1387-3806(00)00400-0

emission per projectile impact, but to generate accurate, sample specific ion signal.

Previous attempts at primary ion comparison looked at the ion formation efficiency, E, which is the yield of a specific secondary ion divided by the disappearance cross section, σ, of that secondary ion [1]. In this article we present a figure-of-merit, which takes into account important factors to be considered for projectile selection. The "projectile efficiency number" (PEN) described in the following is formulated to compare the performance of different primary ions on the same sample.

A comprehensive figure-of-merit must be based on the secondary ion yield from those ions representative of the molecule of interest. Further, it must be modulated for the fragmentation produced by ion bombardment or the amount of sample converted to nonspecific ion signal. Finally, the index must reflect the internal energy content of sputtered secondary ions as a function of primary ion type, for the internal energy content of a secondary ion affects the rate of rearrangement and unimolecular dissociation reactions, i.e. metastable decay, that take place within the mass spectrometer. By examining the extent of metastable decay of a particular secondary ion, a qualitative indication of the change in secondary ion internal energy content as a function of primary ion type can be made. We have combined these three important parameters in the PEN, to produce an indicator of the effectiveness of a primary ion for the analysis of organic samples by static SIMS. Here we compare the PEN values for Cs^+ with those for polyatomic SiF_5^-, $(NaF)_nNa^+$, $(CsI)_nCs^+$, and C_{60}^+ primary ions for the analysis of organic samples prepared as multilayer and monolayer samples.

2. Experimental

2.1. Instrumentation

A dual time-of-flight (TOF) mass spectrometer, described in detail elsewhere [17], was used to acquire the secondary ion mass spectra (Fig. 1). The mass spectrometer was housed in a vacuum chamber

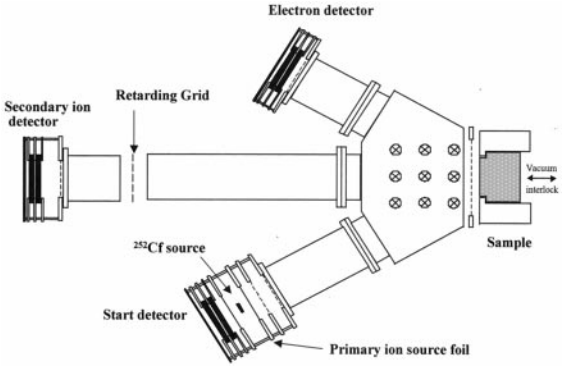

Fig. 1. Diagram of dual-TOF cluster-SIMS instrument.

with a base pressure of $\sim 3 \times 10^{-7}$ Torr. Primary ions were generated with a ^{252}Cf fission fragment source. One of a pair of fission fragments co-emitted from the radioactive ^{252}Cf source was used to produce atomic and polyatomic primary ions from an aluminized Mylar foil that was coated with the source material. The complimentary fission fragment impacted a microchannel plate (MCP) detector located 180° from the Mylar foil, which served as the start signal for the primary ion TOF. Primary ions produced by fission fragment impacts were accelerated to 15 or 20 keV and mass separated in the primary TOF region. The primary ions impact upon a stainless steel cube coated with sample material with an angle of incidence of ~27° with respect to the surface normal. When a primary ion strikes the surface, electrons are emitted and steered with a weak magnetic field to a MCP detector, thereby registering the arrival of a particular primary ion. Sputtered negative secondary ions were then mass analyzed in the 50 cm long secondary TOF region with a mass resolution ($m/\Delta m$) greater than 450.

All experiments were performed in the event-by-event bombardment mode at the limit of single ion impacts. Typical primary ion doses were on the order of 10^5–10^7 ions/cm^2, well within the static SIMS limit (10^{12} ions/cm^2). A coincidence counting data collection approach, developed in our laboratory [13], was used to simultaneously obtain the number of secondary ions sputtered by each primary ion impact. Thus, the transmission and detection efficiencies of the

instrument as well as the target surface conditions remained constant, allowing for direct comparison of the data from all primary ion impacts. Relative secondary ion yields, Y_i, were defined as

$$Y_i = \left(\frac{C_i}{N}\right)(100)$$

where C_i is the area of the secondary ion peak of interest and N is the total number of primary ions that struck the surface.

2.2. Source foil and sample preparation

The following materials were used for generating primary ions: CsI, $NaBF_4$, $(NH_4)_2SiF_6$, (Aldrich Chemical, Milwaukee, WI, USA), and C_{60} (Fluka Chemie AG, Switzerland). Cesium iodide and C_{60} were vapor deposited onto an aluminized Mylar foil to produce $(CsI)_nCs^+$ ($n = 0,1,2$) and C_{60}^+ primary ions. To prepare the SiF_5^- and $(NaF)_nNa^+$ ($n = 0,1,2$) primary ion foils, a 30 μL aliquot of $(NH_4)_2SiF_6$ dissolved in methanol or $NaBF_4$ dissolved in a 50/50 mixture of water and methanol was deposited on an aluminized Mylar foil and dried under a heat lamp.

The organic acid α-cyano-4-hydroxycinnamic acid (ACHA) (Sigma Chemical, St. Louis, MO, USA) was vapor deposited on a stainless steel cube. This produced an organic sample that was infinitely thick relative to the penetration depth of the primary ion. Additional thick targets were prepared by: depositing a 20 μL aliquot of a 0.02 M solution of 1,2-dilauroyl-sn-glycero-3-phosphoethanolamine (DLPE) (Avanti Polar Lipids, Alabaster, AL, USA), depositing a 40 μL aliquot of a 0.0015 M solution of sn-(3-myristoyl-2-hydroxy)-glycerol-1-phospho-sn-3′-(1′-myristoyl-2′-hydroxy)-glycerol (LBPA) (Avanti Polar Lipids, Alabaster, AL, USA), and by depositing a 40 μL aliquot of a 0.01 M solution of octylsulfate (OS) (Aldrich Chemical, Milwaukee, WI, USA) onto a stainless steel cube.

Monolayer targets were prepared following a procedure outlined in [23] and [24]. Briefly, a Si wafer (Wafer World, Inc., W. Palm Beach, FL, USA) was coated with a 10 nm Ti adhesion layer followed by a 200 nm thick Au layer (Lance Goddard Associates, Forest City, CA, USA). This wafer was immersed in a 1 mM solution of 2-aminoethanethiol hydrochloride (Aldrich Chemical, Milwaukee, WI, USA) and ethanol for approximately 18 h. The prepared monolayer was removed from solution, rinsed with ethanol, rinsed with 0.1 M HCl to ensure protonation of the terminal amine, and dried under nitrogen. Next, a 10 μL aliquot of analyte solution was deposited on the protonated monolayer. Analytes used in this study were OS, tetradecylsulfate (TDS) (Aldrich Chemical, Milwaukee, WI, USA), dioctylsulfosuccinate (DSS) (Sigma Chemical, St. Louis, MO, USA), and LBPA. The surface was then rinsed with 50 μL of ethanol for the alkylsulfate samples or 50 μL of chloroform in the case of the phospholipid sample and dried under a stream of nitrogen. This resulted in a surface with sub-monolayer coverage of a preformed negative ion bound to a short chain length monolayer.

2.3. Metastability measurements

If a secondary ion is sputtered with excess internal energy, the ion can undergo a rearrangement or fragmentation reaction in the field free region of a mass spectrometer [25]. If the secondary ion undergoes metastable decay, the parent ion fragments into an ionized fragment and a neutral fragment. The velocity of the ionized and neutral fragments are roughly the same (less any kinetic energy released in the fragmentation reaction) and consequently, the TOF of the ionized and neutral fragments are approximately the same as that of the parent ion. To measure the extent of metastable decay that occurred in the field free region of the instrument, a retarding grid (RG) was placed in the secondary ion TOF region of the mass spectrometer (Fig. 1). Three 2.54 cm aperture plates covered with 90% transmission nickel wire mesh (Buckbee-Mears, St. Paul, MN, USA), were placed 19 cm from the sample (Fig. 1). When the center grid of the RG is grounded, ions and neutral fragments arising from metastable decay are collected in the total secondary ion mass spectrum. However, when an electric potential of −300 V (relative to the acceleration voltage used to extract the secondary

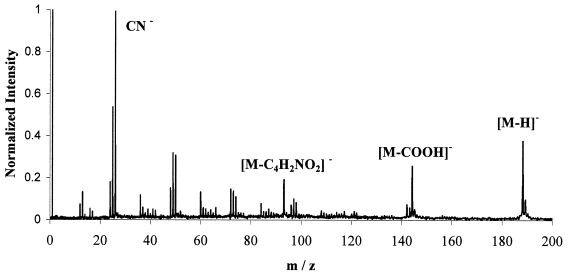

Fig. 2. Mass spectrum of α-cyano-4-hydroxycinnamic acid obtained with 15 keV C_{60}^+ primary ions.

ions) was applied to the center grid of the assembly, all secondary ions are repelled and only neutral molecules arising from metastable decay in the field free region are collected. The decay fraction, D_i, of a particular secondary ion is defined as

$$D_i = \left(\frac{Y_n}{Y_i}\right)(100)$$

where Y_n is the yield of the neutral fragments (RG at −300 V) and Y_i is the yield of the particular secondary ion (RG at ground).

3. Results

3.1. Multilayer sample results

A multilayer target of α-cyano-4-hydroxycinnamic acid (ACHA) was examined to compare the efficiency of different primary ions. Fig. 2 shows the mass spectrum produced by 15 keV C_{60}^+ ion impacts upon ACHA. Secondary ion peaks at *m/z* 189, 144, and 93, corresponding to $[M–H]^-$, $[M–COOH]^-$, and $[M–C_4H_2NO_2]^-$, are characteristic of ACHA (also listed in Table 1). In the mass range of 12–100 amu, note the prominent peaks corresponding to anionic carbon clusters of the form $C_nH_m^-$ ($n = 1, \ldots 8$, $m = 0,1$) as well as the large CN^- peak. Negative carbon clusters are readily produced when organic molecules are analyzed with kiloelectron volt polyatomic primary ions [18,19]. The characteristic secondary ion yields from ACHA produced by 15 keV primary ion impacts are shown in Table 2. As can be seen, relative secondary ion yields for the characteristic ions increase when the atomic primary ion is replaced with a polyatomic primary ion, with $(CsI)Cs^+$ producing the highest yields.

By comparing the yield of the molecular ion to a specific fragment ion yield, Cooks and co-workers [9] showed that a measure of the fragmentation, *F*, produced by a primary ion is revealed by

$$F = \frac{Y_{\text{intact}}}{Y_{\text{frag}}}$$

where Y_{intact} is the yield of an intact ion, in this case $[M–H]^-$, and Y_{frag} is the yield of a molecule specific fragment ion, $[M–C_4H_2NO_2]^-$. The amount of fragmentation that each primary ion produced is shown in Table 3 for each compound studied. For ACHA, Cs^+ primary ions produce almost four times as many deprotonated molecular ions as $[M–C_4H_2NO_2]^-$ fragments. Conversely, C_{60}^+ produces approximately the same amount of each ion. The fragmentation values provide insight into the prompt fragmentation that occurs during desorption and in the acceleration region of the mass spectrometer. To probe the metastable fragmentation that takes place in the field free

Table 1
Characteristic secondary ions from each compound studied

Compound	M.W.	Fragment ions	Intact ion
ACHA	190	*m/z* 93, 144	*m/z* 189
OS	209	*m/z* 80, 96	*m/z* 209
TDS	293	*m/z* 80, 96	*m/z* 293
DSS	424	*m/z* 80, 96	*m/z* 424
DLPE	580	*m/z* 63, 77, 199	*m/z* 579
LBPA	665	*m/z* 63, 77, 227	*m/z* 665

Table 2
Relative secondary ion yields for each compound studied. (x = primary ion not used)

	Multilayer samples					Monolayer samples				
ACHA						OS				
	$[M–C_4H_2NO_2]^-$	$[M–COOH]^-$	$[M–H]^-$				SO_3^-	SO_4^-	M^-	
Cs^+	0.04%	0.09%	0.16%			Cs^+	0.30%	0.08%	1.77%	
$(CsI)Cs^+$	0.46%	0.58%	0.71%			$(CsI)Cs^+$	1.04%	0.44%	2.41%	
$(CsI)_2Cs^+$	0.31%	0.48%	0.52%			$(CsI)_2Cs^+$	1.33%	0.66%	2.82%	
$(NaF)_2Na^+$	0.25%	0.34%	0.46%							
$(NaF)_4Na^+$	0.47%	0.52%	0.63%			TDS				
SiF_5^-	0.31%	0.40%	0.41%				SO_3^-	SO_4^-	M^-	
C_{60}^+	0.44%	0.52%	0.55%			Cs^+	0.17%	0.09%	0.83%	
						$(CsI)Cs^+$	0.44%	0.23%	1.02%	
OS						$(CsI)_2Cs^+$	0.53%	0.31%	0.95%	
	SO_3^-	SO_4^-	M^-							
Cs^+	0.13%	0.09%	0.24%			DSS				
$(CsI)Cs^+$	2.05%	0.66%	3.80%				SO_3^-	SO_4^-	M^-	
$(CsI)_2Cs^+$	3.73%	1.12%	5.98%			Cs^+	1.70%	0.07%	3.79%	
						$(CsI)Cs^+$	3.59%	0.11%	3.34%	
DLPE						$(CsI)_2Cs^+$	3.97%	0.23%	3.07%	
	PO_2^-	PO_3^-	*m/z* 199$^-$	$[M–H]^-$						
Cs^+	0.04%	0.17%	0.13%	0.04%		LBPA				
$(CsI)Cs^+$	0.66%	3.86%	0.83%	0.42%			PO_2^-	PO_3^-	*m/z* 227$^-$	M^-
$(CsI)_2Cs^+$	1.16%	3.95%	0.75%	0.30%		Cs^+	0.12%	0.51%	0.26%	0.20%
C_{60}^+	0.97%	3.20%	0.86%	0.28%		$(CsI)Cs^+$	0.60%	2.84%	0.49%	0.25%
						$(CsI)_2Cs^+$	0.94%	2.78%	0.45%	0.20%
LBPA						$(NaF)Na^+$	0.07%	0.21%	0.11%	0.03%
	PO_2^+	PO_3^-	*m/z* 227$^-$	M^-		$(NaF)_2Na^+$	0.14%	0.61%	0.14%	0.05%
Cs^+	0.04%	0.09%	0.07%	0.01%		$(NaF)_4Na^+$	0.36%	1.51%	0.18%	0.10%
$(CsI)Cs^+$	0.36%	1.35%	0.25%	0.06%		C_{60}^+	0.51%	1.69%	0.23%	0.22%
$(CsI)_2Cs^+$	0.60%	1.59%	0.24%	0.08%						

region of the mass spectrometer, the decay fraction of each of the characteristic ions from ACHA was measured using the RG in the mass spectrometer. The decay fraction of each characteristic secondary ion for ACHA is shown in Table 4. For 15 keV Cs^+ primary ions, only about 6% of the $[M–H]^-$ ions undergo metastable fragmentation (in the time scale of the experiment). Roughly 15% of the $[M–H]^-$ ions undergo metastable decay when 15 keV C_{60}^+ is the projectile, demonstrating that the internal energy of a particular secondary ion can be altered by changing projectile type.

We can now evaluate a primary ion's efficiency by comparing the characteristic secondary ion yield as well as the amount of prompt and metastable fragmentation produced by each primary ion. A PEN can be defined as

$$\text{PEN} = \frac{(\Sigma(Y_i)]F}{\Sigma(D_i)}$$

where ΣY_i is the sum of the yields of characteristic secondary ions (e.g. *m/z* 189, 144, 93) for ACHA, F is the amount of fragmentation, and ΣD_i is the sum of the decay fractions of the characteristic ions. By applying this index to the primary ions used in this study, the PEN values for each primary ion are shown in Fig. 3. The projectile that produces the most characteristic secondary ion yield with minimal fragmentation for ACHA is $(CsI)Cs^+$, which is approximately two times more efficient than a Cs^+ projectile at the same impact energy.

Multilayer samples of OS, DLPE, and LBPA were examined with various primary ions at 20 keV impact energy. Characteristic secondary ions are listed in Table 1 whereas the relative yield of each secondary ion is shown in Table 2. The mass spectrum of OS produces two prominent fragments, SO_3^- and SO_4^-, at *m/z* 80 and *m/z* 96, while the molecular ion for OS

Table 3
Fragmentation value for each compound studied (x = primary ion not used)

	Multilayer samples ACHA	OS	DLPE	LBPA
Cs^+	4.00	1.85	0.31	0.14
$(CsI)Cs^+$	1.54	1.85	0.51	0.24
$(CsI)_2Cs^+$	1.68	1.60	0.40	0.33
$(NaF)_2Na^+$	1.84	*x*	*x*	*x*
$(NaF)_4Na^+$	1.34	*x*	*x*	*x*
SiF_5^-	1.32	*x*	*x*	*x*
C_{60}^+	1.25	*x*	0.33	*x*
	Monolayer samples OS	**TDS**	**DSS**	**LBPA**
Cs^+	5.90	4.88	2.23	0.77
$(CsI)Cs^+$	2.32	2.32	0.93	0.51
$(CsI)_2Cs^+$	2.12	1.79	0.77	0.44
$(NaF)Na^+$	*x*	*x*	*x*	0.27
$(NaF)_2Na^+$	*x*	*x*	*x*	0.36
$(NaF)_4Na^+$	*x*	*x*	*x*	0.56
C_{60}^+	*x*	*x*	*x*	0.96

appears at *m/z* 209. Fragment ions at *m/z* 63, 77, and 199, corresponding to PO_2^-, PO_3^-, and $C_{12}H_{23}O_2^-$ appear in the mass spectrum from DLPE. The deprotonated molecular ion from DLPE is evident at *m/z* 579. Characteristic secondary ions from LBPA are PO_2^-, PO_3^-, and $C_{14}H_{27}O_2^-$, and the $[M–H]^-$ at *m/z* 665. For each sample, a polyatomic primary ion improves the secondary ion yield of the molecular or deprotonated molecular ion versus atomic ion impact. Fragmentation values for OS, DLPE, and LBPA are presented in Table 3. Polyatomic ion bombardment increases fragmentation, as evident by a decrease in the value of the fragmentation factor, for OS consistent with widespread reports of increasing fragmentation for polyatomic ion bombardment. However, for the DLPE and LBPA samples, the amount of fragmentation actually decreases under polyatomic ion bombardment, signifying that the increase in intact ion yield is greater than the increase in fragment ion yield, for polyatomic ion bombardment. The metastable decay of each system was studied and the results are listed in Table 4. Finally, the PEN value for each projectile/sample combination was calculated and the results are given in Table 5. For each sample, a polyatomic primary ion outperforms an atomic primary ion. The five-atom $(CsI)_2Cs^+$ projectile is most effective for OS and LBPA, whereas the three-atom $(CsI)Cs^+$ is most effective for DLPE, illustrating that the most effective primary ion is sample dependent.

3.2. Monolayer sample results

The performance of 20 keV Cs^+, $(CsI)Cs^+$, and $(CsI)_2Cs^+$ was compared for OS, TDS, DSS, and LBPA prepared as monolayer to sub-monolayer thick samples on a 2-aminoethanethiol (AET) monolayer. The mass spectra of TDS and DSS contain SO_3^- and SO_4^- fragment peaks as well as the molecular ion peak at *m/z* 293 for TDS and *m/z* 424 for DSS. The relative yields of each secondary ion are shown in Table 2. For the OS sample, $(CsI)_2Cs^+$ produced the highest molecular ion yield. The molecular ion yield for TDS and LBPA was the greatest for $(CsI)Cs^+$ ion bombardment, whereas Cs^+ primary ions produced the highest yield for the DSS molecular ion. The amount of fragmentation produced by each primary ion (Table 3), was determined using the intact M^- ion and the SO_3^- fragment for the alkyl sulfates, whereas the M^- and $C_{14}H_{27}O_2^-$ ions were used for LBPA. As ex-

Table 4
Decay fractions for each compound studied

	Multi-layer Samples			Monolayer Samples		
ACHA				OS		
	$[M–C_4H_2NO_2]^-$	$[M–COOH]^-$	$[M–H]^-$		M^-	
Cs^+	N.D.	3.93%	5.97%	Cs^+	11.28%	
$(CsI)Cs^+$	1.67%	4.46%	6.22%	$(CsI)Cs^+$	14.92%	
$(CsI)_2Cs^+$	4.81%	9.40%	8.93%	$(CsI)_2Cs^+$	14.31%	
$(NaF)_2Na^+$	1.43%	7.91%	7.08%			
$(NaF)_4Na^+$	0.89%	8.51%	7.54%	TDS		
SiF_5^-	2.54%	3.12%	5.23%		M^-	
C_{60}^-	4.23%	10.63%	14.96%	Cs^+	12.15%	
				$(CsI)Cs^+$	18.92%	
OS				$(CsI)_2Cs^+$	22.08%	
	M^-					
Cs^+	18.64%			DSS		
$(CsI)Cs^+$	16.55%				M^-	
$(CsI)_2Cs^+$	17.89%			Cs^+	20.99%	
				$(CsI)Cs^+$	26.02%	
DLPE				$(CsI)_2Cs^+$	28.76%	
	m/z 199$^-$	$[M–H]^-$				
Cs^+	14.87%	29.38%				
$(CsI)Cs^+$	23.55%	30.17%		LBPA		
$(CsI)_2Cs^+$	28.08%	35.10%			*m/z* 227$^-$	M^-
C_{60}^+	28.43%	44.64%		Cs^+	20.24%	24.39%
				$(CsI)Cs^+$	27.28%	28.11%
LBPA				$(CsI)_2Cs^+$	28.47%	32.33%
	m/z 227$^-$	M^-		$(NaF)Na^+$	15.86%	30.05%
Cs^+	16.81%	28.05%		$(NaF)_2Na^+$	20.50%	28.37%
$(CsI)Cs^+$	24.20%	32.04%		$(NaF)_4Na^+$	27.80%	26.99%
$(CsI)_2Cs^+$	28.25%	26.13%		C_{60}^+	34.05%	31.49%

pected, polyatomic primary ions produced more fragmentation than Cs^+ for the four monolayer samples studied. However, 20 keV C_{60}^+ primary ions produced the smallest amount of fragmentation of any primary ion studied on the LBPA surface.

Decay fraction measurements were also performed for each monolayer sample (Table 4). For each sample, polyatomic primary ion bombardment produced an increase in the amount of metastable decay, compared to Cs^+ projectiles. Molecular ion yield, extent of fragmentation, and decay fraction measurements were used to calculate a PEN value for each primary ion/sample combination (Table 5). The PEN value shows that when a monolayer sample of OS is analyzed, a Cs^+ primary ion is more than twice as effective as a five-atom polyatomic primary ion. Note that the five-atom CsI cluster is equally as effective as the three-atom projectile. The most effective primary ion for a TDS sample is Cs^+ whereas the three-atom CsI cluster is a more effective projectile than the five-atom cluster. For DSS, Cs^+ again has the highest PEN value, indicating that Cs^+ produces a high yield of the molecular ion with minimal prompt and metastable fragmentation. Finally, Cs^+ is more than twice as effective as any polyatomic primary ion when

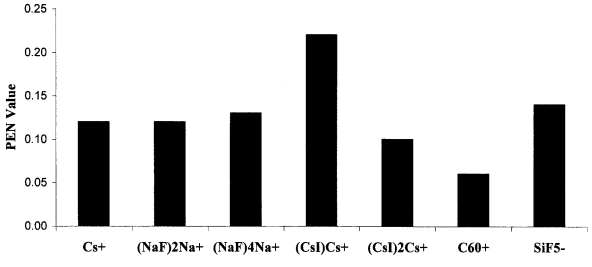

Fig. 3. Projectile efficiency number (PEN) values for each primary ion on ACHA sample.

Table 5
PEN values for each compound studied (x = primary ion not used)

	Multilayer samples			
	ACHA	OS	DLPE	LBPA
Cs^+	0.12	0.02	0.001	2.5×10^{-4}
$(CsI)Cs^+$	0.22	0.42	0.012	0.001
$(CsI)_2Cs^+$	0.10	0.53	0.007	0.002
$(NaF)_2Na^+$	0.12	*x*	*x*	*x*
$(NaF)_4Na^+$	0.13	*x*	*x*	*x*
SiF_5^-	0.14	*x*	*x*	*x*
C_{60}^+	0.06	*x*	0.005	*x*
	Monolayer samples			
	OS	TDS	DSS	LBPA
Cs^+	0.93	0.33	0.40	0.008
$(CsI)Cs^+$	0.37	0.13	0.12	0.007
$(CsI)_2Cs^+$	0.42	0.08	0.08	0.005
$(NaF)Na^+$	*x*	*x*	*x*	8.2×10^{-4}
$(NaF)_2Na^+$	*x*	*x*	*x*	0.001
$(NaF)_4Na^+$	*x*	*x*	*x*	0.003
C_{60}^+	*x*	*x*	*x*	0.007

analyzing LBPA prepared as a monolayer. This comparison demonstrates that the most effective primary ion for routine analysis of monolayer organic samples is an atomic primary ion.

3.3. Multilayer versus monolayer sample comparison

The effect of sample thickness was studied in more detail by comparing a sample of OS prepared as a multilayer sample with one prepared as a monolayer target and comparing a sample of LBPA prepared as a multilayer and a monolayer. For the multilayer sample preparation of OS, a 20 keV $(CsI)_2Cs^+$ projectile improves the molecular ion yield by a factor of 25 compared to Cs^+ ion bombardment (Table 2). However, when the monolayer target was analyzed with $(CsI)_2Cs^+$, the molecular ion yield only increased by a factor of 1.6 versus Cs^+, consistent with other work that shows minimal yield enhancements for monolayer organic surfaces [26,27]. Polyatomic primary ions increase the molecular ion yield of LBPA by a factor of 8 for a multilayer sample but the molecular ion yield increases 1.3 times when a monolayer sample is examined. In Fig. 4(a), the amount of fragmentation produced by each primary ion on the multilayer and monolayer OS sample is shown, whereas Fig. 4(b) shows fragmentation for the multilayer and monolayer samples of LBPA. The decay fraction measurements for the multilayer OS sample and the monolayer sample are shown in Table 4. For the multilayer sample, the three primary ions studied produce approximately the same amount of metastable decay. A comparison of the amount of metastable decay between sample types shows that the amount of metastable decay is lower from the monolayer sample. Additionally, polyatomic primary ions produce more metastable decay than Cs^+ for the monolayer sample. The PEN values for each primary ion on OS are shown in Fig. 5(a), whereas PEN values for the multilayer and monolayer LBPA samples are shown in Fig. 5(b). In each case, a polyatomic primary ion outperforms an atomic primary ion for the bulk organic surface, whereas Cs^+ is the most effective primary ion on the monolayer samples.

4. Discussion

Two variables that influence the effectiveness of a primary ion are the primary ion used and the type of

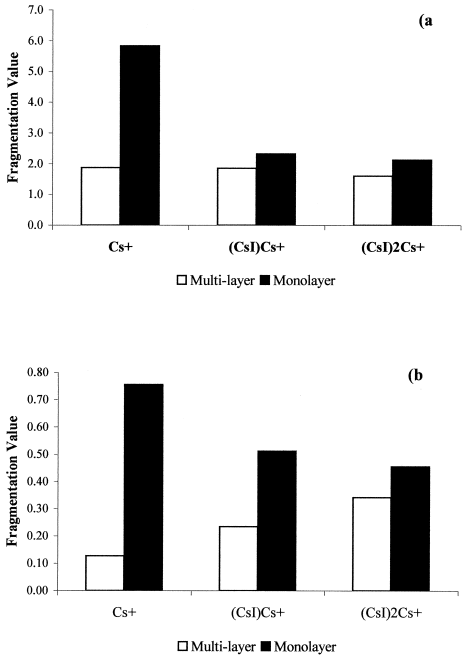

Fig. 4. Fragmentation comparison from (a) OS multilayer sample vs. OS monolayer sample and (b) LBPA multilayer sample vs. LBPA monolayer sample.

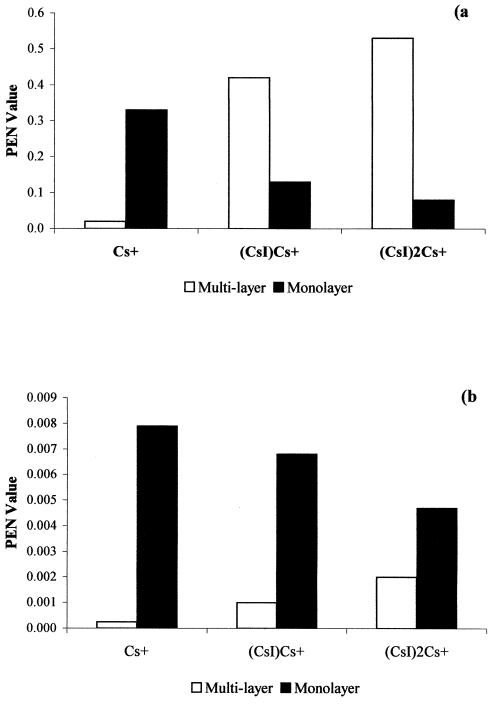

Fig. 5. PEN value comparison for (a) OS multilayer sample vs. OS monolayer sample and (b) LBPA multilayer sample vs. LBPA monolayer sample.

sample that is analyzed. A comparison of the PEN value of each primary ion for the different systems studied shows that depending upon the chemical composition of the analyzed sample, the most efficient projectile changes. For a multilayer sample of ACHA, the most effective primary ion is $(CsI)Cs^+$ whereas a multilayer sample of OS, which is roughly the same molecular weight as ACHA, is best analyzed with $(CsI)_2Cs^+$ projectiles.

Another strong effect on primary ion performance is the sample thickness, in accord with other work [23,26–28]. For OS, large differences in the yield of the molecular ion and the amount of fragmentation are observed depending upon the thickness of the organic sample. Secondary ion yields for a polyatomic primary ion are much higher from a multilayer sample than from a monolayer sample. Recent molecular dynamics simulations [28–30] show that the open nature of an organic solid allows the polyatomic projectile constituents to fragment within the surface and generate collision cascades directed back toward the surface. The model predicts that these backward cascades lead to intact ion emission. Large yield increases with cluster projectiles are typically not observed on thin organic layers upon a metal substrate. It is thought that the polyatomic ion cannot fragment as well within the metal substrate and effectively generate the collision cascades directed towards the surface. For polyatomic ion impacts on a bulk organic solid, the polyatomic projectile can effectively penetrate and fragment within the surface, generating the collision cascades necessary for ion emission.

Fragmentation is also influenced by sample thickness, for the amount of prompt fragmentation from a multilayer sample is much more extensive than from a monolayer sample. The unique sample preparation used in this study can shed some light on this observation. When an ion impacts a surface, it initiates a collision cascade within the solid that leads to desorption and ionization of molecular ions and frag-

ment ions. For an organic solid, the primary ion deposits its kinetic energy within the organic surface causing extensive fragmentation. The monolayers utilized in this study consist of a layer of analyte molecules resting on an AET monolayer approximately 0.5 nm tall, bonded to a gold substrate. When a primary ion strikes this surface, the ion penetrates the analyte and AET layer before depositing the majority of its kinetic energy within the gold substrate. The low coverage and loose packing of the AET monolayer, allow a primary ion to penetrate the organic layer with minimal energy loss. As the collision cascade develops within the Au substrate, Au atoms can be directed back towards the surface. This provides the surface molecule with a concerted push necessary to eject the molecule into the gas phase. Recoiling Au atoms strike the AET molecules, providing the momentum transfer necessary for desorption. Close to the impact site, AET molecules fragment during and after desorption. An analyte molecule bound to a fragmenting AET molecule is provided with the necessary energy for desorption whereas the AET molecule absorbs and dissipates excess energy through fragmentation reactions. This allows the analyte molecule to escape the surface yet undergo little fragmentation.

Another important influence on primary ion performance is the nature of the primary ion. Polyatomic primary ions behave quite differently than atomic primary ions of similar mass. Each atom in a polyatomic projectile initiates a collision cascade upon impact. The collision cascades overlap both spatially and temporally to create a region of high collision density and high energy. Additionally, the kinetic energy of a polyatomic projectile is partitioned between the constituent atoms of the projectile. Each incident atom strikes the surface with only a fraction of the total kinetic energy of the projectile, reducing the penetration depth of the incident ion. For a 15 keV C_{60}^{+} primary ion, each carbon atom will have only 250 eV of kinetic energy. A Sputtering and Range of Ions in Matter calculation [31] of a 250 eV C atom impact on a 0.5 nm thick AET monolayer on a 1000 nm Au substrate, yields a penetration depth of only 1.7 nm. However, a 15 keV Cs atom penetrates to a depth of 4.2 nm. The volume excited by an ion impact can be approximated as the cube of the penetration depth [32], therefore a 15 keV C_{60} projectile will excite a volume that is 15 times smaller than the volume excited by a 15 keV Cs primary ion. Consequently, the energy density (energy per unit volume) will be much higher for a polyatomic ion impact. This region of high energy density and high collision density can be the source for the high amounts of prompt fragmentation seen when a multiatom primary ion is used as a projectile.

One the most important parameters controlling the appearance of the mass spectrum is the internal energy of the sputtered secondary ions. The internal energy of an ion will influence the fragmentation pathways energized as well as the amount of metastable ion dissociation [25]. Previous studies of keV ion bombardment of organic analytes [33] have examined the influence of various parameters on the metastable dissociation of organic secondary ions. The decay fraction results presented here show that the amount of metastable ion dissociation and consequently the internal energy of the secondary ion can be changed by changing the type of primary ion.

Previous attempts at projectile comparison looked at the secondary ion yield and the disappearance cross section, σ, of a particular secondary ion to determine the ion formation efficiency, E [1,4,21,27]. The secondary ion yield measures the number of secondary ions sputtered per primary ion whereas σ measures the average surface area damaged by an ion impact. The disappearance cross-section measures the accumulated damage to the surface in that σ measures the surface area modified so that the secondary ion of interest cannot be generated from this damaged area. Therefore, the ion formation efficiency is a measure of the secondary ions produced from the complete removal of the top one to two layers of the surface.

Our experiment examines the ion yield from discrete ion impacts, with little or no surface modification. The fragmentation values reported in our study are the amount of fragment ions produced from a single ion impact compared to the intact ion yield from a single impact. Although the σ value yields a relative amount of surface area disrupted by an ion

impact, this value is dependent on the type of secondary ion examined. To accurately compare primary ion performance using ion formation efficiency, one has to examine the efficiency for each secondary ion of interest and then evaluate which secondary ion is the most important for the analysis. However, the PEN value incorporates secondary ion yield, fragmentation, and metastable decay into its measurement, yielding one value that summarizes a primary ion's performance allowing for an easy comparison of different primary ions on the same sample.

5. Conclusions

The important parameters for choosing a polyatomic primary ion that will maximize secondary ion yield are the number of atoms in the projectile and the mass of each constituent atom. However, consideration of the amount of fragmentation as well as the amount of metastable decay induced by ion impact is needed to determine which primary ion is best suited for analysis. Through application of the PEN index, this study has confirmed previous results indicating that a polyatomic primary ion is best suited for the analysis of multilayer organic targets. When an organic analyte is prepared as a monolayer, an atomic primary ion (in this case Cs^+) outperforms a polyatomic primary ion. This illustrates the difficulty in making generalizations about which type of primary ion is best suited for analysis. For systems in which a limited amount of sample is dispersed as a single layer, an atomic primary ion is probably sufficient for the analysis. However, if a bulk organic solid, such as a polymer, is to be analyzed, a polyatomic primary ion will provide the highest secondary ion yield. The PEN is an attempt to evaluate primary ion effectiveness on the same sample. As noted earlier, it is not the only way to evaluate primary ion performance. Further, whereas polyatomic primary ions induce more fragmentation than atomic projectiles, this effect could be utilized to provide additional structural information. For instance, a multiatom projectile could be used to access fragmentation pathways previously not accessible under atomic ion bombardment [34].

Acknowledgement

This work was supported by the National Science Foundation (grant no. CHE-9727474).

References

[1] A. Benninghoven, F.G. Rudenauer, H.W. Werner, Secondary Ion Mass Spectrometry, Wiley, New York, 1987, p. 673.
[2] A.D. Appelhans, J.E. Delmore, Anal. Chem. 59 (1987) 1685.
[3] J.F. Mahoney, J. Perel, T.D. Lee, J. Legesse, Int. J. Mass Spectrom. Ion Processes 79 (1987) 249.
[4] A.D. Appelhans, J.E. Delmore, Anal. Chem. 61 (1989) 1087.
[5] M.G. Blain, S. Della-Negra, H. Joret, Y. Le Beyec, E.A. Schweikert, Phys. Rev. Lett. 63 (1989) 1625.
[6] M.G. Blain, S. Della-Negra, H. Joret, Y. Le Beyec, E.A. Schweikert, J. Phys. C2 50 (1989) 147.
[7] J.E. Delmore, A.D. Appelhans, D.A. Dahl, Rev. Sci. Instrum. 61 (1990) 633.
[8] E.A. Schweikert, M.G. Blain, M.A. Park, E.F. da Silveira, Nucl. Instrum. Methods Phys. Res. B 50 (1990) 307.
[9] O.W. Hand, T.K. Majumdar, R.G. Cooks, Int. J. Mass Spectrom. Ion Processes 97 (1990) 35.
[10] J.F. Mahoney, J. Perel, S.A. Ruatta, P.A. Martino, S. Husain, T.D. Lee, Rapid Commun. Mass Spectrom. 5 (1991) 441.
[11] M.A. Park, E.A. Schweikert, E.F. da Silveira, C.V. Barros Leite, J.M.F. Jeronymo, Nucl. Instrum. Methods Phys. Res. B 56/57 (1991) 361.
[12] M. Benguerba, A. Brunelle, S. Della-Negra, J. Depauw, H. Joret, Y. Le Beyec, M.G. Blain, E.A. Schweikert, G. Ben Assayag, P. Sudraud, Nucl. Instrum. Methods Phys. Res. B 62 (1991) 8.
[13] M.A. Park, B.D. Cox, E.A. Schweikert, J. Chem. Phys. 96 (1992) 8171.
[14] P.A. Demirev, J. Eriksson, R.A. Zubarev, R. Papaléo, G. Brinkmalm, P. Håkansson, B.U.R. Sundqvist, Nucl. Instrum. Methods Phys. Res. B 88 (1994) 139.
[15] W. Szymczak, K. Wittmaack, Nucl. Instrum. Methods Phys. Res. B 88 (1994) 149.
[16] K. Boussofiane-Baudin, G. Bolbach, A. Brunelle, S. Della-Negra, P. Håkansson, Y. Le Beyec, Nucl. Instrum. Methods Phys. Res. B 88 (1994) 160.
[17] M.J. Van Stipdonk, R.D. Harris, E.A. Schweikert, Rapid Commun. Mass Spectrom. 10 (1996) 1987.
[18] C.W. Diehnelt, M.J. Van Stipdonk, E.A. Schweikert, Secondary Ion Mass Spectrometry: SIMS XI, G. Gillen, R. Lareau, J. Bennett, F. Stevie (Eds.), Wiley, Chichester, 1998, p. 593.
[19] C.W. Diehnelt, M.J. Van Stipdonk, E.A. Schweikert, Phys. Rev. A 59 (1999) 4470.
[20] G.S. Groenewold, A.K. Gianotto, J.E. Olson, A.D. Appelhans, J.C. Ingram, J.E. Delmore, A.D. Shaw, Int. J. Mass Spectrom. Ion Processes 174 (1998) 129.
[21] F. Kötter, A. Benninghoven, Appl. Surf. Sci. 133 (1998) 47.
[22] G. Gillen, S. Roberson, Rapid Commun. Mass Spectrom. 12 (1998) 1303.

[23] M.J. Van Stipdonk, R.D. English, E.A. Schweikert, J. Phys. Chem. B 103 (1999) 7929.
[24] M.J. Van Stipdonk, R.D. English, E.A. Schweikert, Anal. Chem. 72 (2000) 2618.
[25] F.W. McLafferty, F. Turecek, Interpretation of Mass Spectra, 4th ed., University Science Books, Sausalito, 1993, p. 115.
[26] R.D. Harris, W.S. Baker, M.J. Van Stipdonk, R.M. Crooks, E.A. Schweikert, Rapid Commun. Mass Spectrom. 13 (1999) 1374.
[27] D. Stapel, O. Brox, A. Benninghoven, Appl. Surf. Sci. 140 (1999) 156.
[28] J.A. Townes, A.K. White, E.N. Wiggins, K.D. Krantzman, B.J. Garrison, N. Winograd, J. Phys. Chem. A 24 (1999) 4587.
[29] R. Žarić, B. Pearson, K.D. Krantzman, B.J. Garrison, Int. J. Mass Spectrom. Ion Processes 174 (1998) 155.
[30] D.W. Ward, T.C. Nguyen, K.D. Krantzman, B.J. Garrison, Secondary Ion Mass Spectrometry: SIMS XII, A. Benninghoven, P. Bertrand, H-N. Migeon, H.W. Werner (Eds.), Elsevier, Amsterdam, 2000, p. 183.
[31] J.F. Ziegler, J.P. Biersack, U. Littmark, The Stopping and Ranges of Ions in Solids, J.F. Ziegler (Ed.), Pergamon, New York, 1985, Vol. 1.
[32] B.E. Winger, O.W. Hand, R.G. Cooks, Int. J. Mass Spectrom. Ion Processes 84 (1988) 89.
[33] A. Delcorte, P. Bertrand, Int. J. Mass Spectrom. 184 (1999) 217, and references therein.
[34] C.W. Diehnelt, M.J. Van Stipdonk, R.D. English, E.A. Schweikert, Secondary Ion Mass Spectrometry: SIMS XII, A. Benninghoven, P. Bertrand, H-N. Migeon, H.W. Werner (Eds.), Elsevier, Amsterdam, 2000, p. 179.